Influence of the adhesive thickness on a debonding - An asymptotic model

Azalia Moradi, Dominique Leguillon, Nicolas Carrere

Influence of the adhesive thickness on a debonding – An asymptotic model

A. Moradi [a,b], D. Leguillon [a,*], N. Carrère [c]

[a] *IJLRA, CNRS UMR 7190, Université P. et M. Curie, 4 Place Jussieu, 75252 Paris Cedex, France*
[b] *ONERA/DMSC, 29 avenue de la Division Leclerc, 92322 Châtillon Cedex, France*
[c] *LBMS, ENSTA Bretagne, Université de Brest, 2 rue F. Verny, 29 806 Brest Cedex, France*

The role of the adhesive thickness in the failure of bonded joints is a controversial issue. On the one hand, analytical and numerical models show that the bonding strength is improved as the adhesive thickness increases, on the other hand experimental observations lead to the opposite conclusion. Taking advantage of the thinness of the adhesive layer when com-pared to the overall dimensions of the structure, a matched asymptotic expansions proce-dure allows modeling the initiation of a debonding in a single or double lap joint assembly. If there is a perfect adhesion between the joint and the substrates, the conclusion is iden-tical to the first mentioned. In case of an imperfect bonding, i.e. if there is a micro-crack close to the end of the bonding zone, the trend is reversed and the conclusion meets the experimental observations. Special cases of thick and thin interfaces are highlighted as well as the sensitivity to flaw size.

1. Introduction

Adhesive bonding seems to be a promising way for assembling structural elements in transportation industries. It avoids drilling holes to insert rivets or bolts which induce a drastic reduction of strength due to stress concentrations. However, confidence in this technique must be improved by developing appropriate methods for the prediction of debonding.

Many parameters influence the failure mode and strength of bonded joints [1]. Among these, the role of the adhesive thickness is a controversial issue [2,3]. Analytical models were recently reviewed in [4,5], they predict fracture when stress or strain reaches a maximum in the adhesive. The direct conclusion that emerges is that strength increases with joint thickness. In perfect agreement with these results, FE numerical simulations [6] or cohesive zone models (CZM) [7], allowing the analysis of more complex geometries, lead to the same conclusion, while [8] does not report any thickness effect and [9] notes a trend change according to the values of toughness and tensile strength of the interface.

Unfortunately, these conclusions are inconsistent with experimental observations [10–12], thin joints resist better than thick ones. This disagreement is discussed and well argued in [13]. According to [14], the contradiction between analytical and experimental approaches may be due to voids and micro-cracks that are more prevalent in thick adhesive layers and ignored in the theoretical analysis. Based on fractography observations, another explanation is proposed in [15]: in thin joints both interfaces with the substrates are involved and jumps occur from one to the other whereas only a single one intervenes in thick joints where jumps are inhibited. The ductile behavior of the adhesives is also invoked, coupled either with a plane stress or a plane strain state [4,5], to have a better agreement between analytical and experimental observations. From a numerical viewpoint, the traction-separation law of the CZM used in [16] must be adjusted according to the

* Corresponding author.
E-mail address: dominique.leguillon@upmc.fr (D. Leguillon).

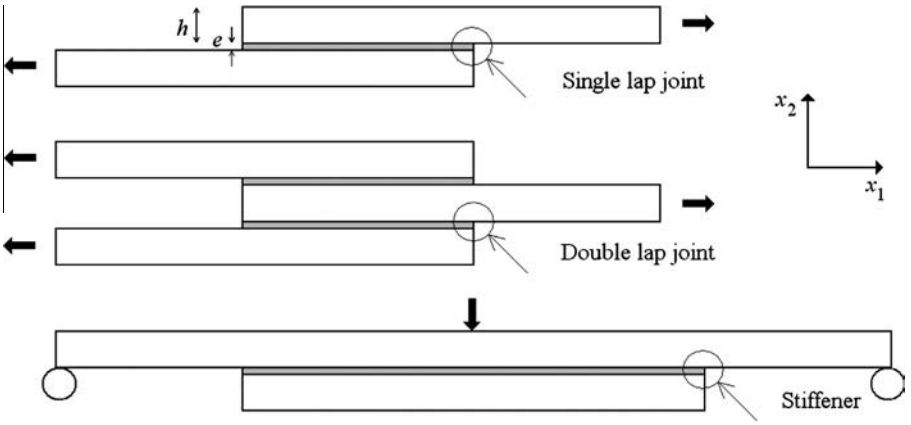

Fig. 1. Traction on a single lap joint assembly, traction on a double lap joint assembly and 3-point bending on a plate with stiffener.

adhesive thickness to render the experimentally observed effects. Based on a Finite Fracture Mechanics approach and analytical expressions for the energy and the stress fields, [17] renders the expected thickness effect.

The previously mentioned analytical models are still a reference for researchers even if they present some limitations, however they are not suitable to take into account models of increasing complexity without integrating a numerical approach. These stress or strain-based models seem to be well appropriate in homogeneous mechanical fields but they rapidly become unsatisfactory in presence of edge effects. The use of an energy criterion issued from the linear elastic fracture mechanics is satisfactory but is appropriate only to predict the propagation of a debonding, not the initiation. So the idea of the so-called coupled criterion [18] consists in mixing the advantages of both stress and energy-based criteria without the drawbacks. Together with a matched asymptotic procedure taking advantage of the smallness of the joint thickness compared to the overall dimensions of the structure, this criterion is used to determine the influence of the adhesive thickness on the strength of a bonded joint. The analysis is performed within the 2D elasticity framework and applies as well to the single and double lap joint configurations or to a stiffened plate (Fig. 1).

2. The asymptotic model

We consider three configurations usually employed to test the strength of a bonded joint between two plates made of the same isotropic elastic material: the traction on a single lap joint assembly, the traction on a double lap joint assembly and the three-point bending on a plate with stiffener (Fig. 1). The thickness e of the adhesive (also assumed isotropic and elastic) is small compared to the thickness of the plates $e \ll h$. It is reasonable to suppose that fracture starts from one of the corners formed by the different assemblies. We focus on those marked with an arrow (Fig. 1) whose local geometry is the same in all cases.

The matched asymptotic expansions approach offers a two-scale description of the specimens. Observed at a large distance (macro-scale), the adhesive layer is no longer visible (Fig. 2). The resulting simplified structures are so-called outer domains, they can be considered in a way as the limit of the actual domains (Fig. 1) as $e \to 0$. Under the assumption of plane strain elasticity, the displacements $\underline{U}^0$ (the index 0 holds for $e = 0$) can be expanded in Williams' series in a vicinity of the corner under consideration as

$$\underline{U}^0(x_1, x_2) = \underline{C} + k_1 r^{\alpha_1} \underline{u}^1(\theta) + k_2 r^{\alpha_2} \underline{u}^2(\theta) + \dots \tag{1}$$

where x_1, x_2 and r, θ are respectively the Cartesian and polar coordinates emanating from the corner tip, they are mixed in the equations throughout this paper without confusion. The leading term $\underline{C}$ is an irrelevant constant. The exponents α_i are solutions to an eigenvalue problem ($0 < \alpha_i < 1$) with the $\underline{u}^i$'s (MPa^{-1}) as eigenvectors [19]. They depend only on the local geometry, typically for a right angle corner in a homogeneous isotropic material $\alpha_1 = 0.545$ and $\alpha_2 = 0.906$ whatever the actual Young modulus and Poisson ratio of the substrates. The coefficients k_1 (MPa m$^{1-\alpha_1}$) and k_2 (MPa m$^{1-\alpha_2}$) are the generalized stress intensity factors (GSIF), they depend on the geometry of the specimens and on the mode and intensity of loading. In the following the second term, corresponding to an exponent close to 1, will be neglected and the index 1 omitted (more precisely, as shown in (3), it is the stress field generated by the omitted terms that is negligible).

$$\underline{U}^0(x_1, x_2) = \underline{C} + k r^{\alpha} \underline{u}(\theta) + \dots \tag{2}$$

According to the elastic constitutive law of the material forming the plates, the expansion for the stress field $\underline{\underline{\sigma}}$ (MPa) can be derived from (2) (the following relation is used to define the tensor $\underline{\underline{s}}$ function of α and θ derived from the singular term exhibited in (2)):

$$\underline{\underline{\sigma}}^0(x_1, x_2) = k r^{\alpha - 1} \underline{\underline{s}}(\theta) + \dots \tag{3}$$

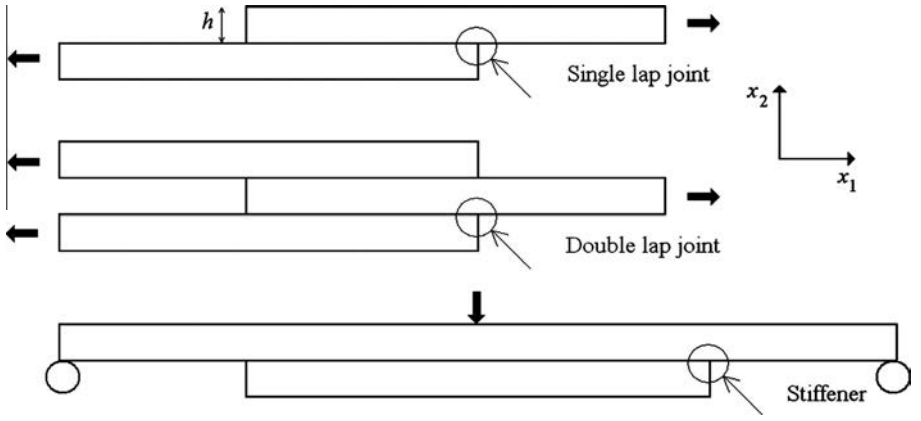

Fig. 2. The outer domains for the three assemblies, the adhesive thickness is no longer visible.

This term is called singular because the associated stress field tends to infinity as $r \to 0$, the exponent α characterizes the stress concentration, smaller the exponent α, stronger the singularity. For a given test (Fig. 1), the GSIF k depends linearly on the intensity of the remote load, in the following it will be denoted remote loading as well.

According to Fig. 2, note that the local geometry is unchanged, thus the same expansions (2) and (3) are valid in the three cases, the GSIF k only changes. It is important to emphasize this point. All the developments that follow are unchanged in all three cases and k is really the only factor, depending on the overall geometry and how the load is applied, which varies from one geometry to another.

The actual solutions depend on e and can be expanded in a so-called outer expansion

$$\underline{U}^e(x_1,x_2) = \underline{U}^0(x_1,x_2) + \text{small correction} \tag{4}$$

The small correction is assumed to tend to zero with the adhesive thickness e, it does not play any role in the forthcoming analysis.

After zooming-in ($\times 1/e$) near the corner under consideration, the global geometry of the specimens is no longer visible but details (the adhesive thickness here) are highlighted (Fig. 3), it is the micro-scale. The corresponding domain is called the inner domain, it is spanned by the dimensionless variables $y_i = x_i/e$ ($\rho = r/e$), the adhesive thickness is now 1 and the domain becomes unbounded as $e \to 0$.

In this domain, the actual solutions are expanded in a so-called inner expansion

$$\underline{U}^e(x_1,x_2) = \underline{U}^e(ey_1,ey_2) = F_0(e)\underline{V}^0(y_1,y_2) + F_1(e)\underline{V}^1(y_1,y_2) + \dots \tag{5}$$

Using the change of variables mentioned above it is easy to write the equilibrium and constitutive equations as well as the boundary conditions on the two faces of the corner for the successive terms $\underline{V}^i$. Nevertheless, conditions prescribing behavior at infinity are missing, they are provided by the matching rules between inner (5) and outer (4) expansions. Together with (1) they give

$$F_0(e) = 1; \quad \underline{V}^0(y_1,y_2) \sim \underline{C}; \quad F_1(e) = ke^{\alpha}; \quad \underline{V}^1(y_1,y_2) \sim \rho^{\alpha}\underline{u}(\theta) \tag{6}$$

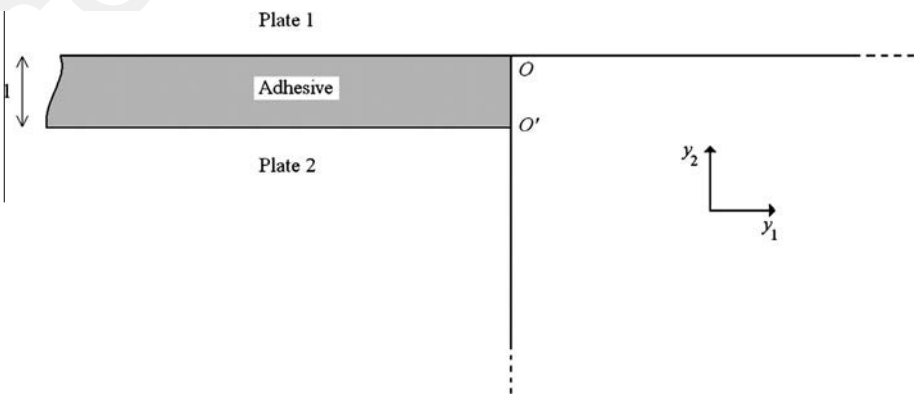

Fig. 3. The common inner domain spanned by y_1, y_2.

Here $\sim$ means "behaves like at infinity". And finally (5) can be written using a superposition principle

$$\underline{U}^e(x_1,x_2)=\underline{U}^e(ey_1,ey_2)=\underline{C}+ke^{\alpha}\underline{V}^1(y_1,y_2)+\ldots \quad \text{with } \underline{V}^1(y_1,y_2)=\rho^{\alpha}\underline{u}(\theta)+\hat{\underline{V}}^1(y_1,y_2) \tag{7}$$

It is not possible to solve directly for $\underline{V}^1$ (MPa^{-1}) because of its behavior at infinity, it grows indefinitely like ρ^{α} (see (6)) and thus has not a finite energy in the inner domain. It is necessary to proceed by superposition $(7)_2$, where $\hat{\underline{V}}^1$ tends to 0 at infinity. However, the well-posedness of the problem for $\hat{\underline{V}}^1$ is not obvious. The external forces in the variational formulation of the problem in $\hat{\underline{V}}^1$ involve integrals within the unbounded thin adhesive layer and along its interfaces. Roughly, they converge because the polar angle θ within the layer behaves like $1/\rho$ as ρ tends to infinity.

In must be pointed out that $\underline{V}^1$ undergoes a singularity at O (and another at O' but weaker and disregarded, Fig. 3) and can be expanded in a Williams series

$$\underline{V}^1(y_1,y_2)=\underline{C}^1+\kappa\rho^{\beta}\underline{V}(\theta)+\ldots \tag{8}$$

Only one singular exponent β is retained since the second one is often larger than 1 in this particular case where the lower material (the adhesive) is more compliant than the upper one (the upper plate) (Fig. 3). Unlike α, β depends on the elastic contrast between the plates and the adhesive. The GSIF κ is dimensionless and independent of the global geometry and the remote applied loads. Plugging (8) into (5) and using (6) lead to

$$\underline{U}^e(x_1,x_2)=\ldots+\kappa ke^{\alpha-\beta}r^{\beta}\underline{V}(\theta)+\ldots=\ldots+Kr^{\beta}\underline{V}(\theta)+\ldots \quad \text{with} \quad K=\kappa ke^{\alpha-\beta} \tag{9}$$

The actual GSIF K (MPa m$^{1-\beta}$) of the singularity at the corner between the adhesive and the upper layer depends on the GSIF k (function of the remote loading) and the adhesive thickness e. The relationship between k and K in (9) provides a matching condition between the two a priori incompatible singularities characterized by the exponents α and β.

3. Crack initiation at the corner – the coupled criterion

In addition, we assume now that there is a short crack with length l starting from the corner and lying along the upper interface because this is the most likely location for the initiation of rupture. Beside we assume that l is much smaller than h ($l \ll h$). So there are now two small parameters e and l and if one of them is not infinitely smaller or larger than the other (see Sections 4 and 5), asymptotic expansions can be carried out relatively to one or the other leading to strictly equivalent results from the theoretical point of view.

From afar (outer domain), neither crack length nor adhesive thickness are visible, thus Williams' expansion (2) and outer expansion (4) are unchanged.

For practical reasons, it is more convenient to use again e as the small parameter involved in the asymptotics and to consider the crack length as an additional variable

$$\underline{U}^e(x_1,x_2,l)=\underline{U}^0(x_1,x_2)+\text{small correction} \tag{10}$$

In the inner domain the dimensionless crack length is $\mu = l/e$ (Fig. 4), and it is quite easy to vary this length by buttoning/unbuttoning the nodes along the crack path in a conventional FE computation.

The inner expansion (7) can be written

$$\underline{U}^e(x_1,x_2,l)=\underline{U}^e(ey_1,ey_2,e\mu)=\underline{C}+ke^{\alpha}[\rho^{\alpha}\underline{u}(\theta)+\hat{\underline{V}}^1(y_1,y_2,\mu)]+\ldots \tag{11}$$

The change in potential energy δW between an initial sound state and a final one embedding a short crack can be calculated using the path independent integral Ψ

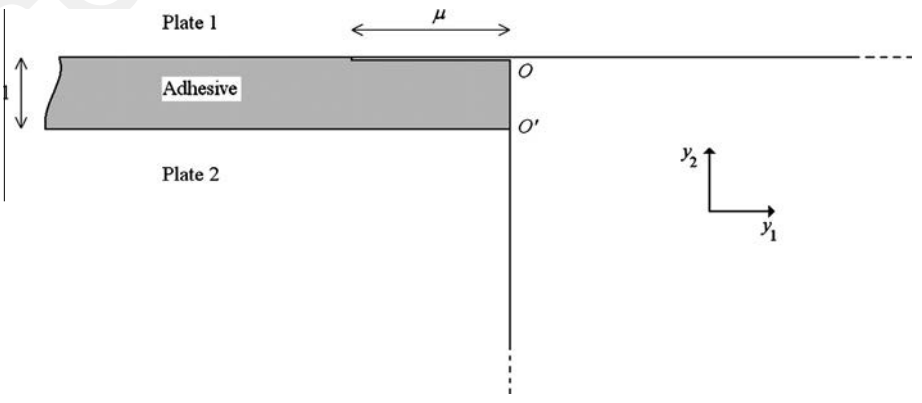

Fig. 4. The inner domain spanned by y_1, y_2 with a short crack along the upper interface.

$$\delta W = \Psi(\underline{U}^e(x_1,x_2,l\ ),\underline{U}^e(x_1,x_2,0))$$
$$\text{with by definition } \Psi(\underline{f},\underline{g}) = \tfrac{1}{2}\int_\Gamma (\underline{\underline{\sigma}}(\underline{f}).\underline{N}.\underline{g} - (\underline{\underline{\sigma}}(\underline{g})).\underline{N}.\underline{f})\mathrm{d}s \tag{12}$$

where Γ is any contour encompassing the corner and the new crack and $\underline{N}$ its normal pointing toward the origin [19,20]. This integral can be computed either in the outer or in the inner domain. Plugging (11) into (12) gives

$$\delta W = k^2 e^{2\alpha}(A(\mu) - A(0))t + \ldots \tag{13}$$

Here t holds for the specimen width (plane strain assumption) and the function $A(\mu)$ is extracted from $\underline{V}^1$ [21]

$$A(\mu) = \Psi(\underline{V}^1(y_1,y_2,\mu), \rho^\alpha \underline{u}(\theta)) \tag{14}$$

The change in potential energy must be compared with the fracture energy $G_c lt$ where G_c (MPa mm) is the interface toughness and lt the newly created crack surface. A necessary condition for the nucleation of a short crack straightforwardly derives from an energy balance

$$k^2 e^{2\alpha-1}\frac{A(\mu) - A(0)}{\mu} \geqslant G_c \tag{15}$$

This inequality provides a lower bound for the admissible dimensionless crack lengths μ. Indeed we should be more precise on the definition of G_c, is it G_{Ic}, i.e. the mode I toughness, or do we have to take into account mode mixity? At this step let us take $G_c = G_{Ic}$ arguing that at the very beginning of onset the crack is almost in an opening mode [22].

It has been shown that such a crack nucleation cannot be described by a sole energetic argument, two conditions must be fulfilled simultaneously: one based on energy and involving the material toughness as above and another based on stress and involving the material strength [18]. We are going to exploit this statement to describe the initiation of the debonding.

Prior to crack nucleation, using the elastic constitutive law, (7) and (11), it comes

$$\underline{\underline{\sigma}}(x_1,x_2) = \mathbf{C} : \nabla_x \underline{U}^e(x_1,x_2,0) = k e^{\alpha-1}\underline{\underline{\tilde{\sigma}}}(y_1,y_2) + \ldots \quad \text{with } \underline{\underline{\tilde{\sigma}}}(y_1,y_2) = \mathbf{C} : \nabla_y \underline{V}^1(y_1,y_2,0) \tag{16}$$

where $\mathbf{C}$ is the elastic tensor either of the material forming the plates or of the adhesive depending on the location x_1, x_2 of the point, ∇_x and ∇_y the gradient operators with respect to the x_i's and y_i's.

The stress condition states that failure occurs if the tensile stress component σ (MPa) acting on the interface is greater than the tensile strength σ_c (MPa) of the interface all along the pre-supposed crack path (as explained previously, initiation being mainly in opening mode, σ_c is the out-of-plan tensile strength)

$$\sigma(x_1,0) \geqslant \sigma_c \text{ for } -l \leqslant x_1 \leqslant 0 \Rightarrow \sigma(-l,0) \geqslant \sigma_c \quad \text{or equivalently} \quad k e^{\alpha-1}\tilde{\sigma}(-\mu,0) \geqslant \sigma_c \tag{17}$$

It should be noted that single or double lap joint experiments are often considered as testing the shear strength. It is true when dealing with the study of the growth of a pre-existing long crack at the interface but wrong for crack initiation where the opening mode I dominates. This was observed in [22,23]. Moreover, the shear stress often does not play a big role in a fracture process except when mode II becomes much predominant and when the shear failure parameters are low [24,25].

Since σ is a decreasing function of the distance to the corner in its vicinity, the inequality (17) provides an upper bound for the admissible values of μ.

For small loadings (i.e. small k) the conditions (15) and (17) are incompatible. Increasing the load leads to a value of μ for which the two inequalities are just fulfilled

$$\frac{1}{\tilde{\sigma}(-\mu,0)^2}\frac{A(\mu) - A(0)}{\mu} = \frac{1}{e}\frac{G_c}{\sigma_c^2} \tag{18}$$

Let μ_c be the solution to (18), then the remote load at failure $k_c^{(g)}$ ((g) holds for general) is characterized by

$$k = k_c^{(g)} = \left(\frac{\mu_c G_c}{A(\mu_c) - A(0)}\right)^{1-\alpha}\left(\frac{\sigma_c}{\tilde{\sigma}(-\mu_c,0)}\right)^{2\alpha-1} \tag{19}$$

As claimed in [18] the crack initiation is a discontinuous process, the crack jumps the length $l_c = \mu_c e$.

4. Particular case 1: a short crack jump (thick adhesive)

If the crack length l is very small compared to the adhesive thickness $l \ll e$ ($\mu \ll 1$), the crack in the inner domain (Fig. 4) can be considered as a small perturbation of the uncracked case (Fig. 3) and the matched asymptotic procedure can be iterated. The "outer" expansion of $\underline{V}^1$ is (it is an outer expansion in the space spanned by y_1, y_2)

$$\underline{V}^1(y_1,y_2,\mu) = \underline{V}^1(y_1,y_2,0) + \text{small correction} \tag{20}$$

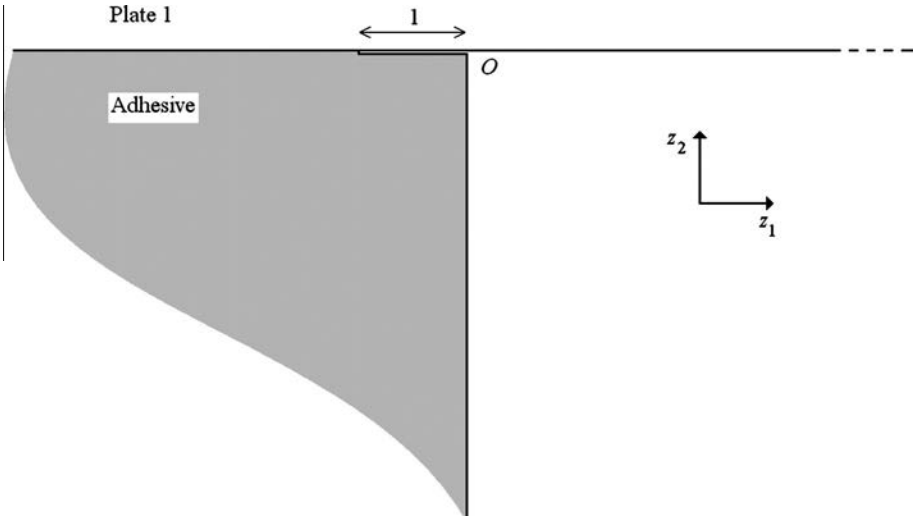

Fig. 5. The inner domain spanned by z_1, z_2.

And the Williams expansion of the leading term is given by (8). A new zooming-in ($\times 1/\mu$) can be carried out and a new unbounded (as $\mu \to 0$) secondary inner domain spanned by z_1, z_2 ($z_i = y_i/\mu$, $\zeta = \rho/\mu$) is defined (Fig. 5), it could be baptized "inner inner". The new inner expansion can be written

$$\underline{V}^1(y_1, y_2, \mu) = \underline{V}^1(\mu z_1, \mu z_2, \mu) = G_0(\mu)\underline{W}^0(z_1, z_2) + G_1(\mu)\underline{W}^1(z_1, z_2) + \dots \tag{21}$$

With the previous notations, the new matching conditions are

$$G_0(\mu) = 1; \quad \underline{W}^0(z_1, z_2) \sim \underline{C}^1; \quad G_1(\mu) = \kappa\mu^\beta; \quad \underline{W}^1(z_1, z_2) \sim \zeta^\beta \underline{v}(\theta) \tag{22}$$

Then

$$\underline{V}^1(y_1, y_2, \mu) = \underline{V}^1(\mu z_1, \mu z_2, \mu) = \underline{C}^1 + \kappa\mu^\beta \underline{W}^1(z_1, z_2) + \dots \quad \text{with} \quad \underline{W}^1(z_1, z_2) = \zeta^\beta \underline{v}(\theta) + \hat{\underline{W}}^1(z_1, z_2) \tag{23}$$

Using again (12), the integral is now computed in the secondary inner domain and all calculations gives

$$\delta W = k^2\kappa^2 e^{2(\alpha-\beta)} l^{2\beta} B t + \dots \quad \text{with} \quad B = \Psi(\underline{W}^1(z_1, z_2), \zeta^\beta \underline{v}(\theta)) \tag{24}$$

And the energy condition becomes

$$k^2\kappa^2 e^{2(\alpha-\beta)} l^{2\beta-1} B \geqslant G_c \tag{25}$$

With an obvious generalization of the previous notations (see (16)) the stress field can be written

$$\underline{\sigma}(x_1, x_2) = k\kappa e^{\alpha-\beta} l^{\beta-1} \underline{\tilde{\sigma}}(z_1, z_2) + \dots \quad \text{with} \quad \underline{\tilde{\sigma}}(z_1, z_2) = \mathbf{C} : \nabla_z(\zeta^\beta \underline{v}(\theta)) \tag{26}$$

The stress condition for failure is

$$k\kappa e^{\alpha-\beta} l^{\beta-1} \tilde{\sigma}(z_1, 0) \geqslant \sigma_c \quad \text{for} \quad -1 \leqslant z_1 \leqslant 0 \Rightarrow k\kappa e^{\alpha-\beta} l^{\beta-1} \tilde{\sigma}(-1, 0) \geqslant \sigma_c \tag{27}$$

Knowing that, prior to crack nucleation (the following relation is used to define the tensor $\underline{\tau}$ function of β and θ derived from the singular term exhibited in (8) and (22))

$$\underline{\tilde{\sigma}}(z_1, z_2) = \mathbf{C} : \nabla_z(\zeta^\beta \underline{v}(\theta)) = \zeta^{\beta-1} \underline{\tau}(\theta) \tag{28}$$

It comes finally

$$k\kappa e^{\alpha-\beta} l^{\beta-1} \tau(\theta_0) \geqslant \sigma_c \tag{29}$$

where θ_0 is the angular abscissa of the interface and τ the tensile component of $\underline{\tau}$. Bringing together (25) and (29), and using (9) allow writing the coupled criterion as

$$l_c = \frac{G_c}{B}\left(\frac{\tau(\theta_0)}{\sigma_c}\right)^2 \quad \text{and} \quad K = k\kappa e^{\alpha-\beta} = K_c = \left(\frac{G_c}{B}\right)^{1-\beta}\left(\frac{\sigma_c}{\tau(\theta_0)}\right)^{2\beta-1} \tag{30}$$

At this step, it is essential to check the validity of the initial assumption: is l_c far smaller than e? It is clear that this will be true if G_c is small and σ_c is big enough. Relation (30) is important, since k can be identified with the remote load intensity, remote load at failure $k_c^{(s)}$ ((s) holds for short) depends on the adhesive thickness as

$$k_c^{(s)} = \frac{K_c}{\kappa} e^{\beta-\alpha} \tag{31}$$

Thus, if $\alpha < \beta$ the critical load at failure increases with the thickness while conversely, it decreases if $\alpha > \beta$ [23].

5. Particular case 2: a long crack jump (thin adhesive)

This particular case is easier to treat. If the crack jump l is large compared to e ($l \gg e$), let us carried out the matched asymptotics (4) and (5) with respect to l instead of e. The outer expansion (4) and the Williams expansion (2) are unchanged. After the change of variables $\tilde{y}_i = x_i/l (\tilde{\rho} = r/l)$, the inner expansion takes obviously the form

$$\underline{U}^e(x_1,x_2,l) = \underline{U}^e(l\tilde{y}_1,l\tilde{y}_2,l) = \underline{C} + kl^{\alpha}\underline{\tilde{V}}^1(l\tilde{y}_1,l\tilde{y}_2,1/\mu) + \ldots \quad \text{with} \quad \underline{\tilde{V}}^1(l\tilde{y}_1,l\tilde{y}_2,1/\mu) = \tilde{\rho}^{\alpha}\underline{u}(\theta) + \underline{\hat{\tilde{V}}}^1(l\tilde{y}_1,l\tilde{y}_2,1/\mu) \tag{32}$$

In the inner domain (Fig. 6), the dimensionless adhesive thickness $1/\mu$ is small ($1/\mu \ll 1$) and can be considered as a perturbation of a homogeneous inner domain and then the "outer" expansion for $\underline{\tilde{V}}^1$ is

$$\underline{\tilde{V}}^1(l\tilde{y}_1,l\tilde{y}_2,1/\mu) = \underline{\tilde{V}}^1(l\tilde{y}_1,l\tilde{y}_2,0) + \text{small correction} \tag{33}$$

The energy and stress conditions now read (s is the tensile component of $\underline{s}$, see (3))

$$k^2 l^{2\alpha-1}\tilde{A} \geqslant G_c; \quad kl^{\alpha-1}s(\theta_0) \geqslant \sigma_c \quad \text{with} \quad \tilde{A} = \Psi(\underline{\tilde{V}}^1(\tilde{y}_1,\tilde{y}_2,0),\tilde{\rho}^{\alpha}\underline{u}(\theta)) \tag{34}$$

Leading to a classical form of the coupled criterion [18]

$$l_c = \frac{G_c}{\tilde{A}}\left(\frac{s(\theta_0)}{\sigma_c}\right)^2; \quad k = k_c^{(l)} = \left(\frac{G_c}{\tilde{A}}\right)^{1-\alpha}\left(\frac{\sigma_c}{s(\theta_0)}\right)^{2\alpha-1} \tag{35}$$

Again, validity of the reasoning is guaranteed if l_c is by far larger than e ($l_c \gg e$). That can be achieved if G_c is large and σ_c is small. So, as expected these conditions are exactly opposite to those of the previous particular case.

Here, everything goes as if one could ignore the presence of the adhesive, except for the determination of the interface parameters G_c and σ_c of course. The critical load at failure is almost independent of the adhesive thickness.

6. Numerical tests

In this section, we try to verify that the particular cases of Sections 4 and 5 are the two limits of the general case covered by Section 3. The different terms of the expansions are computed using a conventional FE code and simple linear elements. The unbounded inner domains are artificially bounded at a large (compared to the perturbation size) distance and the behaviors at infinity of the different inner terms are prescribed along this fictitious line. The Ψ integral is calculated using a home-made post-processing. The parameters and functions involved in the singular terms of the Williams expansion are numerically obtained using again a home-made code.

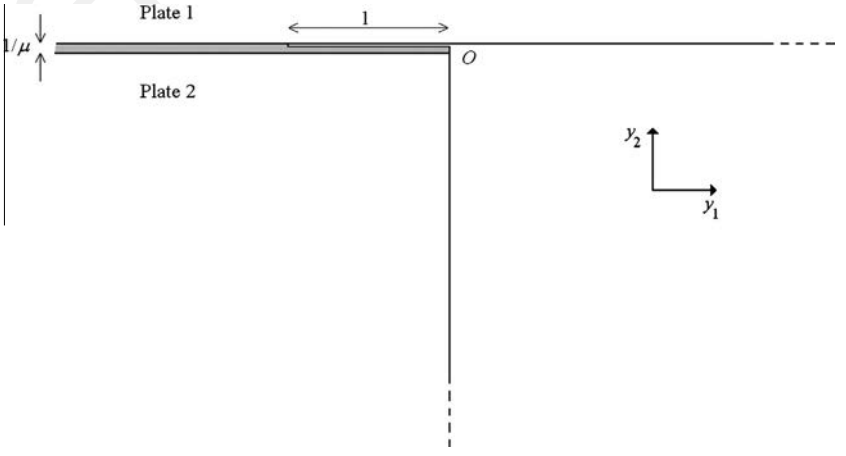

Fig. 6. The inner domain spanned by $\tilde{y}_1$, $\tilde{y}_2$ when $l \gg e$.

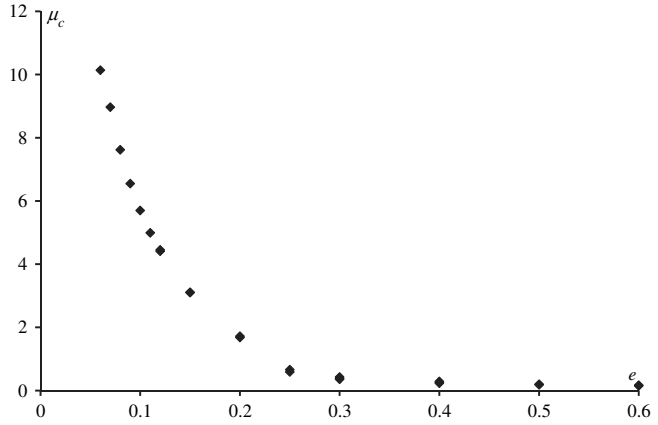

Fig. 7. The relative crack jump μ_c vs. the adhesive thickness e (mm). Superposed diamonds correspond to different meshes used to treat both short and long cracks.

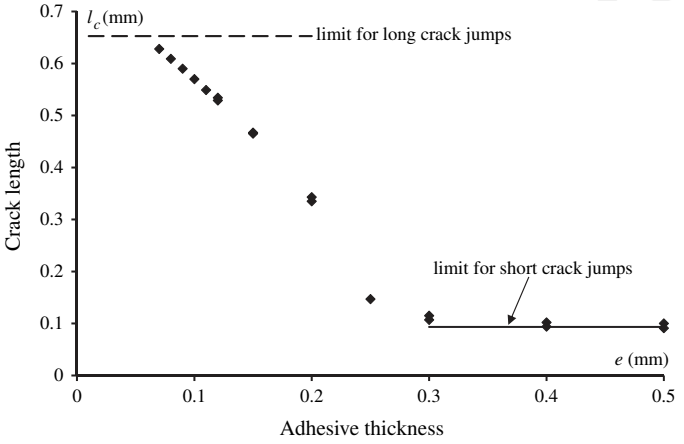

Fig. 8. The crack jump length $l_c = \mu_c e$ (Eq. (18)) (mm) (diamonds) vs. the adhesive thickness e (mm), the solid line corresponds to l_c for short jumps (Eq. (30)) and the dashed one to l_c for long jumps (Eq. (35)). Superposed diamonds correspond to different meshes used to treat both short and long cracks.

To be realistic, the Young moduli contrast between the plates and the adhesive is taken equal to 0.04, resulting in $\alpha = 0.545$ (already mentioned in Section 2) and $\beta = 0.692$. This contrast can vary considerably from 0.5 for a brazed assembly of Silicon Carbide rods [26] to 0.01 for the bonding of steel plates with an epoxy adhesive [5,23]. To fix the ideas 0.04 corresponds to $E_p = 70{,}000$ MPa (like glass or aluminum) and $E_a = 2800$ MPa (an epoxy resin), where E_p and E_a hold respectively for the Young moduli of the plates and the adhesive [27,28]. For simplicity, the Poisson ratios are the same in the two materials $\nu_p = \nu_a = 0.3$ and close to the actual values, within a reasonable range (say 0.1–0.4) results do not change a lot. The interface toughness is $G_c = 0.15$ MPa mm and the tensile strength $\sigma_c = 50$ MPa, these values correspond roughly to bulk parameters of adhesives [5,27,28]. Here these values are also assigned to the interface implying a perfect bonding; however, they can be significantly lower when the interface is imperfect and especially when the surfaces are not treated [29].

Fig. 7 shows the dimensionless crack length μ_c solution to (18) as a function of the adhesive thickness e, thicker the adhesive and smaller the relative crack jump. We found that for $e < 0.06$ mm $\mu_c > 10$ (i.e. $l_c > 0.6$ mm) and for $e > 0.9$ mm (out of the range of Fig. 7) $\mu_c < 0.1$ ($l_c < 0.09$ mm) out of these adhesive thickness bounds 0.06–0.9 mm, the crack length l can no longer be considered of the same order than the adhesive thickness, it is either far larger or far smaller. As a consequence thick adhesives ($e > 0.9$ mm and $l_c < 0.09$ mm) enter in the particular case studied in Section 4 (short crack jump) and vice versa thin adhesives ($e < 0.06$ mm and $l_c > 0.6$ mm) are studied in Section 5 (long crack jump). The corresponding physical crack jump length $l_c = e\mu_c$ is illustrated in Fig. 8. The convergences toward one of the above cases at the two ends of the thickness domain are clearly visible.

The critical load at failure k_c is calculated in the three cases: the complete model (Eq. (19) in Section 3), the short crack jump case (thick adhesive) (Eq. (31) in Section 4) and the long crack jump case (thin adhesive) (Eq. (35) in Section 5). For a short crack, the value of κ is required, it is extracted from $\underline{V}^1(y_1, y_2)$ using again the Ψ integral (12)

$$\kappa = \frac{\Psi(\underline{V}^1(y_1, y_2), \rho^{-\beta}\underline{v}^-(\theta))}{\Psi(\rho^{\beta}\underline{v}(\theta), \rho^{-\beta}\underline{v}^-(\theta))} \tag{36}$$

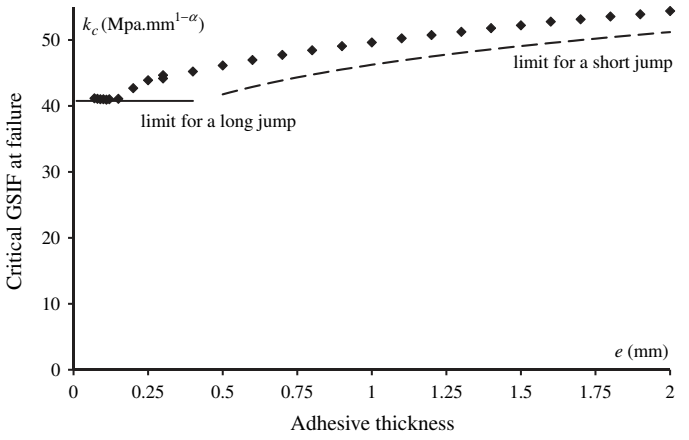

Fig. 9. The critical load at failure k_c (MPa mm$^{1-\alpha}$) vs. the adhesive thickness e (mm): complete model (diamonds) (Eq. (19)), short jump (dashed line) (Eq. (31)), long jump (solid line) (Eq. (35)).

It is shown in [19] that the Ψ integral can be used both for the calculation of the potential energy change or for the calculation of the GSIF's. In the first case, the extraction function (second argument of Ψ) has a positive exponent (see (12)–(14)) and in the second a negative one (see (36)). The second use of Ψ is based on the peculiar following property: if β is one solution of the eigenvalue problem, then $-\beta$ is too with its own eigenvector $\underline{v}^-(\theta)$ [19].

One can note that the convergence is not really numerically guaranteed for short cracks, the complete calculations (diamonds) overestimate the limit case (dashed line) roughly by 6%. Indeed, when μ is decreasing and becoming small, calculations are more difficult to achieve because, due to the buttoning procedure, there are less and less free nodes along the crack in the inner domain, resulting in a reduced accuracy.

Fig. 9 shows that if long jumps occur (thin adhesive), the critical load at failure is almost insensitive to the adhesive thickness. At the other end of the thickness range, the critical load at failure increases with the adhesive thickness according to (31) since $\beta > \alpha$. This result is in agreement with other analytical or numerical approaches cited in Section 1. It is not completely surprising since thick adhesive layers release the tensile stress better than thin ones. But, as already claimed (Section 1), this result is inconsistent with experiments where it is shown that the critical failure load decreases as the adhesive thickness increases.

Note that in Fig. 9 the adhesive thickness varies from 0 to 2 mm, this final thickness is large in practical cases, but it must remain small compared to the thickness h of the substrate to ensure the validity of the asymptotic expansions.

7. A pre-existing flaw in the vicinity of the corner

As already emphasized, the main drawback of the above approach is that it is inconsistent with experiments where it is observed that thicker the layer and less resistant the assembly at least for thick adhesive layers. The reason is that $\beta > \alpha$ in (31). To overcome this drawback let us suppose that there is a lack of bonding along the interface near the corner. A crack with length l_0 ($\mu_0 = l_0/e$) is located at a short distance d_0 ($\delta_0 = d_0/e$) of the corner (Fig. 10). Both l_0 and d_0 are known and

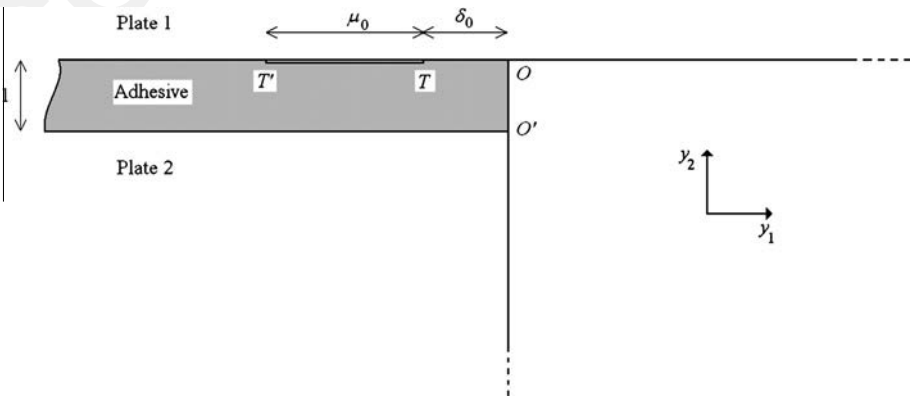

Fig. 10. A short flaw with dimensionless length $\mu_0 = l_0/e$ along the interface at a short distance $\delta_0 = d_0/l$ of the corner.

assumed to be of the same order of magnitude than e (i.e. μ_0 and δ_0 close to 1). Statistically these micro-cracks are present throughout the interface, but their role is enhanced in the vicinity of the end of the joint, due to stress concentrations at this location, we neglect the interaction between them.

Under this assumption Williams' expansion (2) and outer expansion (4) are unchanged. The inner domain spanned by y_1, y_2 is illustrated in Fig. 10. The inner expansion is almost the same as (7) where $\underline{V}^1$ and $\hat{\underline{V}}^1$ now depend on μ_0 and δ_0

$$\begin{aligned}\underline{U}^e(x_1,x_2,l_0,d_0) &= \underline{U}^e(ey_1,ey_2,e\mu_0,e\delta_0) = \underline{C} + ke^{\alpha}\underline{V}^1(y_1,y_2,\mu_0,\delta_0) + \ldots \quad \text{with} \quad \underline{V}^1(y_1,y_2,\mu_0,\delta_0) \\ &= \rho^{\alpha}\underline{u}(\theta) + \hat{\underline{V}}^1(y_1,y_2,\mu_0,\delta_0)\end{aligned} \tag{37}$$

The fracture problem has now a slightly different nature, it is no longer the study of a crack nucleation in a sound material but the growth of a pre-existing crack. This crack has two tips located at T and T' and $\underline{V}^1$ can be expanded in the vicinity of these points using the classical Williams expansion near the tip of an interface crack [30]. They are similar at the two ends and only one (say at T') is presented (they are analogous to (9), ρ' and θ' denote the polar coordinates emanating from T')

$$\underline{V}^1(y_1y_2,\mu_0,\delta_0) = \ldots + \chi\rho'^{1/2+i\varepsilon}\underline{w}(\theta') + \bar{\chi}\rho'^{1/2-i\varepsilon}\bar{\underline{w}}(\theta') + \ldots \tag{38}$$

Here, the exponent is complex with a real part 1/2 and an imaginary part ε depending on the contrast between the materials [31] (here $\varepsilon = 0.087$), the associated eigenvector $\underline{w}$ is complex as well, the upper bar denotes the complex conjugate. The complex dimensionless stress intensity factor (SIF) χ depends on μ_0 and δ_0. According to (37), the actual complex SIF X of the interface crack tip singularity at T' is

$$X = ke^{\alpha-1/2-i\varepsilon}\chi \tag{39}$$

The energy release rate (ERR) G at the crack tip can be written [30,32]

$$G = DX\bar{X} = Dk^2e^{2\alpha-1}\chi\bar{\chi} \tag{40}$$

where D is a real coefficient. Following the Griffith criterion, the pre-existing crack grows if

$$G \geqslant G_c \Rightarrow k \geqslant k_c^{(f)} = \sqrt{\frac{G_c}{D\chi\bar{\chi}}}\, e^{1/2-\alpha} \tag{41}$$

Now the role of the adhesive thickness e is reversed ($1/2 - \alpha < 0$) and more consistent with experimental observations.

Note that in this section, it is not necessary to use the coupled criterion because the exponent, although complex, has a real part equal to 1/2 and in this case the criterion merges with Griffith's. To understand this point just look at the more simple case (30) with $\beta = 1/2$ (similar to a complex exponent with a real part 1/2). One sees immediately that the second term that involves the tensile strength disappears and it remains a Griffith criterion under the Irwin form (i.e. a critical value of the stress intensity factor).

8. Flaw at the corner – numerical simulations

To illustrate the previous section, a simplified model is treated: $l_0 = e/2$ and $d_0 = 0$. The flaw is directly located at the corner with a dimensionless length $\mu_0 = 1/2$ (Fig. 11). This choice has been done purely to give an example. The vanishing ligament width allows simplifying the calculations and reduces the number of parameters. The flaw size l_0 is arbitrarily selected to be small but not far smaller than the adhesive thickness.

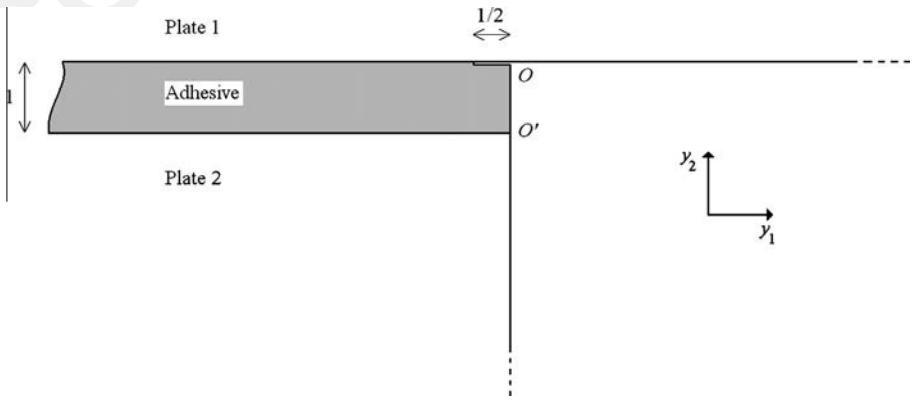

Fig. 11. A zoom-in of the flaw at the corner (inner domain, $\mu_0 = 1/2$).

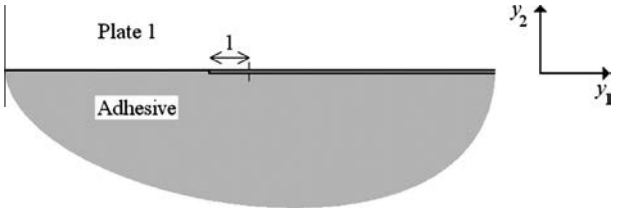

Fig. 12. The unbounded inner domain to analyze the crack growth along an interface.

Although some quantities such as ε and D are analytically known [30], we have chosen to use the numerical approach developed in [19] which then facilitates the calculation of the complex SIF χ. All the procedures initially planned for real calculations can be formally extended and still work in complex including the integral Ψ defined in (12). There is no additional theoretical difficulties, the obstacles are purely of a technical nature and related to more complicated expressions.

Unlike a crack kinking out of an interface [33], the rectilinear propagation along the interface is fairly easier to analyze. Computing D requires solving, by superposition as before, a (real) problem in the inner domain illustrated in Fig. 12. The solution $\underline{Z}$ must fulfil the classical equilibrium equations and boundary conditions on the two crack faces and, due to the matching rules, the prescribed behavior at infinity is

$$\underline{Z}(y_1, y_2) \sim \mathrm{Re}(\rho^{1/2+i\varepsilon}\underline{w}(\theta)) \tag{42}$$

Then

$$D = 4\Psi(\underline{Z}(y_1, y_2), \mathrm{Re}(\rho^{1/2+i\varepsilon}\underline{w}(\theta))) \tag{43}$$

The inner term $\underline{V}^1$ (or $\hat{\underline{V}}^1$ see (7)) is solved in the domain defined in Fig. 11 instead of that of Fig. 3. Then, as in Section 6, the complex SIF χ is computed using the path independent integral Ψ (see (36)) which still works for complex functions

$$\chi = \frac{\Psi(\underline{V}^1(y_1, y_2), \rho'^{-1/2-i\varepsilon}\underline{w}^-(\theta'))}{\Psi(\rho'^{1/2+i\varepsilon}\underline{w}(\theta'), \rho'^{-1/2-i\varepsilon}\underline{w}^-(\theta'))} \tag{44}$$

Note that the SIF χ as well as D depend on the choice made to normalize the complex eigenvector $\underline{w}$, but of course, the final result leading to G (see (40)) no longer depends on this choice.

With the material data of Section 6, we get $D = 0.075$ (MPa^{-1}) and $\chi = 0.265 + i\,0.162$. A comparison of the critical load at failure $k_c^{(f)}$ (41) with its counterpart $k_c^{(g)}$ (19) in case of a sound bonding is shown in Fig. 13. The trend reversal related to the role of the adhesive thickness is visible, the critical load increases in the sound case while it decays in the presence of a defect.

Except for thin adhesive layers, in presence of the defect of size $l_0 = e/2$ the load at failure is lower than that of the sound bonding, this means that the assembly is sensitive to this flaw size.

In (41) and in Fig. 13, the smallest value the slope of the curve can reach is obtained for $\alpha = 1$, i.e. when there is no stress concentration. Then the critical load at failure behaves like $1/\sqrt{e}$. This is achieved for instance for an interface flaw far from the ends of the adhesive layer or at the ends of a butt joint [26].

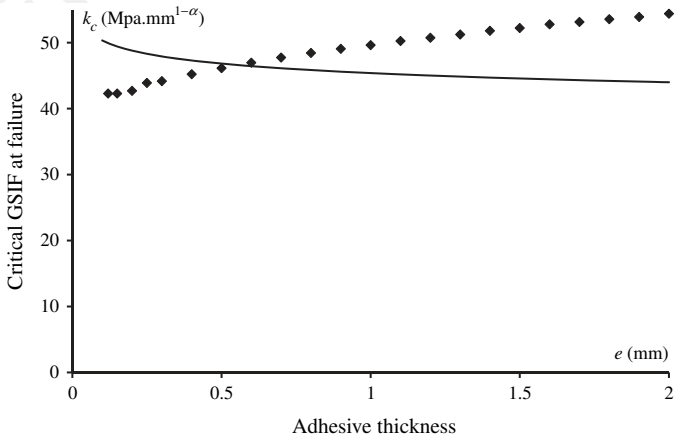

Fig. 13. Comparison of the critical load at failure of a sound adhesive bonding (diamonds, (Eq. (19)) and an imperfect bonding (solid line, Eq. (41)).

Table 1
Elastic and fracture parameters of the substrates and the adhesive and singularity exponent at the corners steel/steel (Fig. 2) and steel/adhesive (Fig. 3) [12,17].

	E	ν	σ_c	G_c	α	β
Steel	210,000	0.3				
AV138	4590 (MPa)	0.35	41 (MPa)	0.38 (MPa mm)	0.545	0.671

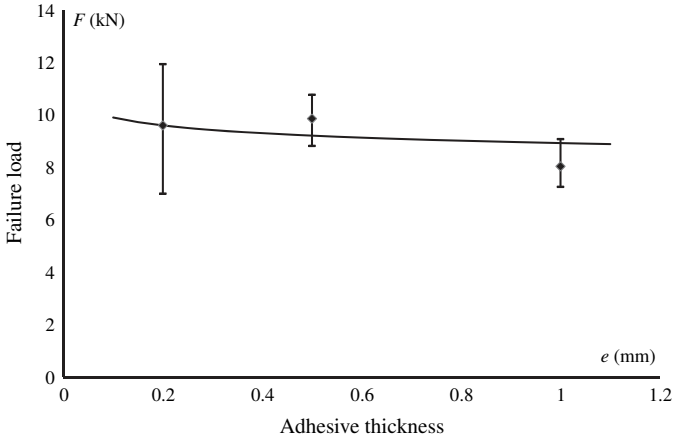

Fig. 14. Comparison of the experimental failure load F (kN) (diamonds and error bars) [12], with the predicted one (solid line) according to (45) and Table 2 for AV138/HV998.

However, one should be extremely careful in the interpretation of Fig. 13, the flaw length l_0 varies with the thickness e, therefore the observed decay of the solid line takes into account two effects: the trend reversal and a growth of the flaw size with the thickness. A simple way to confirm the validity of relationship (41) is to compare with experiments found in [12] on a single lap assembly of steel plates. Steel plates are bonded together using the brittle adhesive Araldite AV138/HV998 from Huntsman. Nevertheless, in the present reference, the adhesive thickness e (0.2, 0.5 and 1 mm) cannot really be considered as small compared to the arms thickness h (2 mm) at least in the two last cases. Indeed, the smallness assumption has emerged from a theoretical point of view to ensure the validity of the asymptotic expansions. It is clear that when the ratio falls below 0.05 a good accuracy can be expected from the approach. It is still satisfactory when this ratio is 0.1 and the formulas (frequently the only available) are often used for even larger values (0.25) in the hope that the error remains still reasonable.

The elastic and failure properties are shown in Table 1 with the corresponding singularity exponent at the corner steel/adhesive (Fig. 3).

Let us denote F (kN) the failure load, according to (41), the generic form of the relation between failure load and adhesive thickness is

$$F = \frac{\Lambda}{e^{\alpha-1/2}} \tag{45}$$

The coefficient Λ (it has no special physical meaning except to be a scaling coefficient between the thickness and the load at failure) is identified on the first experimental point $e = 0.2$ mm and Fig. 14 shows a satisfactory agreement knowing that the adhesive AV 138 is reported to be very brittle. The adhesive EA 9361 is ductile and EA 9321 intermediate and the matching between experiments and predictions are not so good. Note that there are only two available measures apart that used for identification and it is obviously not enough to conclude definitively. Moreover, it is clear that the asymptotic assumption of smallness of the adhesive thickness compared to the two arms thicknesses (2 mm) is no longer valid for $e = 0.5$ mm and a fortiori for $e = 1$ mm. The goal is simply to show the trend reversal and a good agreement of this trend with the experimental observations not to provide an accurate prediction of the mechanism.

9. Sensitivity to defects

We only consider the simplified case of Section 8, i.e. a short crack with length l_0 emanating directly from the corner ($d_0 = 0$, Fig. 11).

Table 2
The flaw size sensitivity in case of a thin adhesive layer.

e (mm)	0.05	0.075	0.1	0.125	0.15	0.175	0.2
l_0 (mm)	0.016	0.020	0.027	0.033	0.038	0.042	0.047

On the one hand χ changes a little for large flaw sizes (but still small compared to the overall dimensions of the structure). If l_0 varies from $e/2$ to 5 e, χ increases slowly from 0.265 + i 0.162 ($\chi\bar{\chi} = 0.096$) to 0.260 + i 0.198 ($\chi\bar{\chi} = 1.07$). Thus according to (41), remote load at failure depends mainly on the adhesive thickness and is almost insensitive to the flaw size.

On the other hand, smaller the flaw size and higher the failure load. If $\mu_0 \ll 1$ (say $\mu_0 < 0.1$ or less) following an analogous reasoning to that of Section 4 leads to

$$\chi = \kappa \mu_0^{\beta-1/2-i\varepsilon}\eta \tag{46}$$

where η is the complex SIF of the interface crack tip singularity in the inner domain spanned by z_1, z_2 (Fig. 5)

$$\eta = \frac{\Psi(\underline{W}^1(z_1,z_2), \zeta^{-1/2-i\varepsilon}\underline{w}^-(\theta))}{\Psi(\zeta^{1/2+i\varepsilon}\underline{w}(\theta), \zeta^{-1/2-i\varepsilon}\underline{w}^-(\theta))} \tag{47}$$

Plugging (46) into (41) and using the definition of μ_0 leads to

$$k_c^{(f)} = \frac{1}{l_0^{\beta-1/2}}\frac{e^{\beta-\alpha}}{\kappa}\sqrt{\frac{G_c}{D\eta\bar{\eta}}} \tag{48}$$

Obviously, the remote load at failure $k_c^{(f)}$ increases indefinitely when l_0 diminishes, thus it can reach values that are not eligible because higher than the remote load at failure $k_c^{(g)}$ obtained in the absence of defect. It is difficult to carry out the comparison directly with $k_c^{(g)}$ involving μ_c which is only implicitly known as the solution to (18), but it can be done in the two particular cases of Sections 4 and 5.

If the adhesive layer is thick (Section 4), the model is insensitive to flaw size smaller than the following value

$$l_0^{\beta-1/2} \leqslant \frac{1}{K_c}\sqrt{\frac{G_c}{D\eta\bar{\eta}}} \Rightarrow l_0 \leqslant 0.083 \text{ mm} \tag{49}$$

where K_c is given by (30) and η = 0.902 + i 0.276. The initial assumption $\mu_0 << 1$ allows estimating the validity range of (49) to $e > 0.8$ mm, while remaining smaller than h.

If the adhesive layer is thin (Section 5), it comes

$$l_0^{\beta-1/2} \leqslant \frac{e^{\beta-\alpha}}{\kappa k_c^{(l)}}\sqrt{\frac{G_c}{D\eta\bar{\eta}}} \tag{50}$$

where $k_c^{(l)}$ is given by (35). The limit flaw size depends now on the adhesive thickness e and is given in Table 2.Thicker the adhesive layer and larger the flaw size tolerance, (49) is a limit value (independent of e) and it is possible to interpolate between this limit and Table 2 for intermediate thicknesses.

Note that this result is debatable because the initial assumption $\mu_0 \ll 1$ setting the asymptotic validity of (46) is not strictly true. We must once again hope that this result is not too affected by errors.

10. Conclusion

To achieve a model consistent with experimental observations, the need for taking into account defects along the interface to predict initiation of debonding was evidenced in this work. Models of a perfect adhesion between the joint and the substrates leads usually to a bonding reinforcement with increasing adhesive layer thickness, in disagreement with experiments, whereas models based on an imperfect adhesion with micro-cracks leads to the opposite conclusion which is in a better agreement with experiments. The main result lies in relationship (41) between the remote load at failure and the adhesive thickness, consequences are shown in Figs. 13 and 14. When the defect size becomes very small the flawless case is recovered. This allows introducing the concept of sensitivity to defects. The threshold below which a flaw has no longer any influence on the remote load at failure depends on the thickness of the joint, thinner the joint and higher the sensitivity (i.e. smaller the flaw size threshold). It should be emphasized that the notion of adhesive thinness is relative and closely related to the values of G_c and σ_c (see (18)). Joints are classified as thick or thin if G_c is small and σ_c is big enough or vice versa.

Acknowledgements

The collaboration with SNECMA is gratefully acknowledged. This work was supported under the PRC Composites, French research project funded by DGAC, involving SAFRAN Group, ONERA and CNRS.

References

[1] da Silva LFM, Carbas RJC, Critchlow GW, Figueiredo MAV, Brown K. Effect of material, geometry, surface treatment and environment on the shear strength of single lap joints. Int J Adhes Adhes 2009;29:621–32.
[2] Azari S, Papini M, Spelt JK. Effect of adhesive thickness on fatigue and fracture of toughened epoxy joints – Part I: experiments. Engng Fract Mech 2011;78:153–62.
[3] Azari S, Papini M, Spelt JK. Effect of adhesive thickness on fatigue and fracture of toughened epoxy joints – Part II: analysis and finite element modelling. Engng Fract Mech 2011;78:138–52.
[4] da Silva LFM, das Neves PJC, Adams RD, Spelt JK. Analytical models of adhesively bonded joints – Part I: literature survey. Int J Adhes Adhes 2009;29:331–41.
[5] da Silva LFM, das Neves PJC, Adams RD, Wang A, Spelt JK. Analytical models of adhesively bonded joints – Part II: Comparative study. Int J Adhes Adhes 2009;29:319–30.
[6] Ouinas D, Bouiadjra BB, Achour T, Benderdouche N. Influence of disbond on notch crack behaviour in single bonded lap joints. Mater Des 2010;31:4356–62.
[7] Xu W, Wei Y. Strength and interface failure mechanism of adhesive joints. Int J Adhes Adhes 2012;34:80–92.
[8] Choupani N. Characterization of fracture in adhesively bonded double-lap joints. Int J Adhes Adhes 2009;29:761–73.
[9] Moradi A, Carrère N, Martin E, Leguillon D, Cognard JY. Strength prediction of bonded assemblies using a coupled criterion under elastic assumptions: effect of geometrical parameters. Int J Adhes Adhes 2013;47:73–82.
[10] Adams RD, Comyn J, Wake WC. Structural adhesive joints in engineering. 2nd ed. London: Chapman and Hall; 1997.
[11] da Silva LFM, Adams RD, Gibbs M. Manufacture of adhesive joints and bulk specimens with high-temperature adhesives. Int J Adhes Adhes 2004;24:69–83.
[12] da Silva LFM, Rodrigues TNSS, Figueiredo MAV, de Moura MFSF, Chousal JAG. Effect of adhesive type and thickness on the lap shear strength. J Adhes 2006;82:1091–115.
[13] Gleich DM, Van Tooren MJL, Beukers A. Analysis and evaluation of bondline thickness effects on failure load in adhesively bonded structures. J Adhes Sci Technol 2001;15:1091–101.
[14] Adams RD, Peppiatt NA. Stress analysis of adhesively bonded lap joints. J Strain Anal 1974;9:185–96.
[15] Taib AA, Boukhili R, Achiou S, Gordon S, Boukehili H. Bonded joints with composite adherends. Part I. Effect of specimen configuration, adhesive thickness, spew fillet and adherend stiffness on fracture. Int J Adhes Adhes 2006;26:226–36.
[16] Xu W, Wei Y. Influence of the adhesive thickness on local interface fracture and overall strength of metallic adhesive bonding structures. Int J Adhes Adhes 2013;40:158–67.
[17] Weissgraeber P, Becker W. Finite fracture mechanics model for mixed mode fracture in adhesive joints. Int J Solids Struct 2013;50:2383–94.
[18] Leguillon D. Strength or toughness? A criterion for crack onset at a notch. Eur J Mech – A/Solids 2002;21:61–72.
[19] Leguillon D, Sanchez-Palencia E. Computation of singular solutions in elliptic problems and elasticity. New York: John Wiley & Son; 1987.
[20] Labossiere PEW, Dunn ML. Stress intensities at interface corners in anisotropic bimaterials. Engng Fract Mech 1999;62:555–75.
[21] Leguillon D, Quesada D, Putot C, Martin E. Prediction of crack initiation at blunt notches and cavities – size effects. Engng Fract Mech 2007;74:2420–36.
[22] Braccini M, Dupeux M, Leguillon D. Initiation of failure in a single lap joint. In: Proceedings in conference Int Conf on fracture ICF XI, Torino, Italy; March 20–25, 2005 (CD-ROM).
[23] Leguillon D, Laurencin J, Dupeux M. Failure initiation in an epoxy joint between two steel plates. Eur J Mech A/Solids 2003;22:509–24.
[24] Tran VX, Leguillon D, Krishnan A, Xu LR. Interface crack initiation at V-notches along adhesive bonding in weakly bonded polymers subjected to mixed-mode loading. Int J Fract 2012;176:65–79.
[25] Garcia IG, Leguillon D. Mixed-mode crack initiation in presence of an adhesive joint. Int J Solids Struct 2012;49:2138–49.
[26] Nguyen LM, Leguillon D, Gillia O, Riviere E. Bond failure of a SiC/SiC brazed assembly. Mech Mater 2012;50:1–8.
[27] Caimmi F, Pavan A. An experimental evaluation of glass-polymer interfacial toughness. Engng Fract Mech 2009;76:2731–47.
[28] Park JH, Choi JH, Kweon JH. Evaluating the strengths of thick aluminium-to-aluminium joints with different adhesive lengths and thicknesses. Comp Struct 2010;92:2226–35.
[29] Krishnan A, Xu LR. Systematic evaluation of bonding strengths and fracture toughnesses of adhesive joints. J Adhes 2011;87:1–19.
[30] Rice JR. Fracture mechanics concepts for interfacial cracks. J Appl Mech 1988;55:98–103.
[31] Dundurs J. Effect of elastic constants on stress in a composite under plane deformation. J Comp Mater 1967;1:310–23.
[32] Leguillon D. Calcul du taux de restitution de l'énergie au voisinage d'une singularité. CR Acad Sci Paris 1989;309(II):945–50.
[33] Leguillon D, Murer S. A criterion for crack kinking out of an interface. Key Engng Mater 2008;385–387:9–12.